Particle and pair spectra for strongly correlated Fermi gases: A real-frequency solver

Tilman Enss
Institut für Theoretische Physik, Universität Heidelberg, 69120 Heidelberg, Germany

(Received 14 November 2023; accepted 23 January 2024; published 21 February 2024)

The strongly attractive Fermi gas in the BCS-BEC crossover is efficiently described in terms of coupled fermions and fermion pairs, or molecules. We compute the spectral functions of both fermions and pairs in the normal state near the superfluid transition using a Keldysh formulation in real frequency. The mutual influence between fermions and pairs is captured by solving the self-consistent Luttinger-Ward equations: These include both the damping of fermions by scattering off dressed pairs and the decay of pair states by dissociation into two dressed fermions. The pair spectra encode contact correlations between fermions and form the basis for computing dynamical response functions and transport properties.

DOI: 10.1103/PhysRevA.109.023325

I. INTRODUCTION

Strongly correlated Fermi gases are ubiquitous in nature and appear in very diverse physical realizations ranging from ultracold atomic gases [1,2] to dilute nuclear matter [3]. In their theoretical description, however, universality provides a framework to reveal the common features of these systems. Recent experimental advances in atomic spectroscopy have brought the dynamical properties and even transport within reach of high-precision measurements [4].

In dilute yet strongly attractive Fermi gases, pair fluctuations play a dominant role throughout the BCS-BEC crossover [5]. Not only do they describe the condensation of fermion pairs in the low-temperature superfluid state, but virtual pair fluctuations also strongly renormalize the properties of the normal state above the superfluid transition temperature T_c [6–8]. Pair fluctuations alone, however, are not sufficient, and density (particle-hole) fluctuations lead to a substantial reduction of T_c at weak coupling [9]. Also at resonant scattering in the unitary regime [1], the value of $T_c \simeq 0.16T_F$ from experiment [10] and quantum Monte Carlo [11] is very well reproduced in field-theoretic approaches based on the self-consistent T-matrix approximation or Luttinger-Ward theory [12–15] (for related self-consistent GW approaches see [16]). This approach includes particle-hole fluctuations in the fermion and pair self-energies, which are computed self-consistently at one-loop order with fully dressed propagator lines. Diagrammatic Monte Carlo results confirm that further multiloop contributions modify the density equation of state by less than 10% even at T_c [17].

In these approaches, the coupled self-consistent equations for fermions and pairs have been solved numerically in imaginary (Matsubara) frequency or time. This is computationally convenient because convergence properties are well understood. However, real-frequency spectra can only be obtained by analytical continuation, which is mathematically ill-defined and requires exponential precision in imaginary frequency to obtain reliable real-frequency data. Exponential precision, however, is not achievable in numerical self-consistent solutions. We therefore propose to solve the self-consistent equations directly in real frequency, which circumvents analytical continuation. We present an algorithm that computes fermion spectra and self-consistent pair spectra reliably even with standard numerical precision. As we explain below, the main idea is to represent the fermion and pair self-energies as slowly varying functions interpolated on a real-frequency and momentum grid and then use analytical integration between grid points to obtain highly accurate spectra that capture also sharp spectral features much narrower than the grid spacing.

This paper is structured as follows. In Sec. II we introduce the Keldysh formulation of the strongly correlated Fermi gas in equilibrium. The self-consistent solution in real frequency is developed in Sec. III. In Sec. IV we present the resulting fermion and pair spectra for the strongly correlated three-dimensional Fermi gas in the BCS-BEC crossover. We conclude in Sec. V and discuss how these results can form the basis for future self-consistent computations of dynamical response functions and transport directly in real frequency.

II. FERMI GAS MODEL IN THE KELDYSH FORMULATION

A. Attractive Fermi gas

We consider a two-component Fermi gas in three dimensions, which is described by the Hamiltonian

$$H = \sum_\sigma \int d\boldsymbol{r}\, \psi_\sigma^\dagger(\boldsymbol{r})\left(-\frac{\hbar^2\nabla^2}{2m} - \mu_\sigma\right)\psi_\sigma(\boldsymbol{r}) + g_0 \int d\boldsymbol{r}\, \psi_\uparrow^\dagger(\boldsymbol{r})\psi_\downarrow^\dagger(\boldsymbol{r})\psi_\downarrow(\boldsymbol{r})\psi_\uparrow(\boldsymbol{r}). \tag{1}$$

Here $\psi_\sigma(\boldsymbol{r})$ denotes the field operator for a fermion of species $\sigma = \uparrow, \downarrow$ and mass m at chemical potential μ_σ. The second term represents an attractive contact interaction between unlike fermions of bare strength $g_0 < 0$. The contact interaction needs to be regularized at short distance in two and higher dimensions, and in three dimensions it is related to the low-

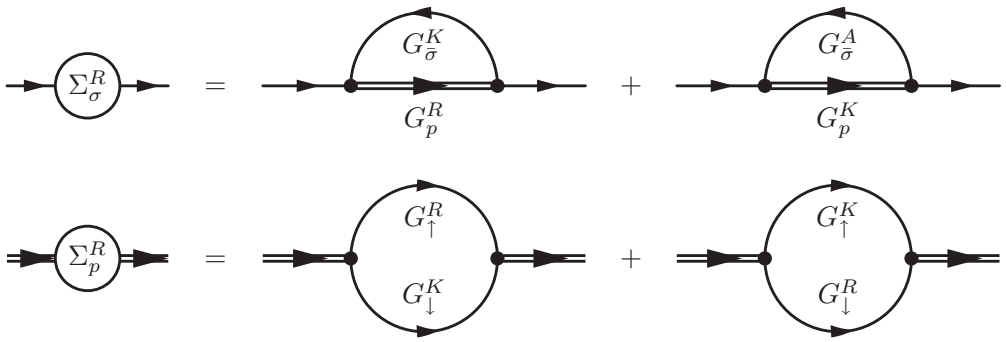

FIG. 1. Feynman diagrams for the fermionic and pair self-energies in Keldysh formulation, with G^R (retarded), G^A (advanced), and G^K (Keldysh) propagators. All propagator lines are bold and represent fully dressed fermions (single) and pairs (double lines).

energy s-wave scattering length a via

$$\frac{1}{g_0} = \frac{m}{4\pi\hbar^2 a} - \frac{m\Lambda}{2\pi^2\hbar^2} \tag{2}$$

in the presence of a large-wave-number cutoff Λ. The attractive interaction tends to form pairs of fermions, and for positive scattering length $a > 0$ there exists a bound state of two fermions at a binding energy of

$$E_b = \frac{\hbar^2}{ma^2} > 0. \tag{3}$$

Even when the attraction is too weak to form a bound state at negative scattering length $a < 0$, virtual pair fluctuations play an important role. It is therefore natural to introduce a local pair field

$$\Delta(\boldsymbol{r}) = g_0\psi_\downarrow(\boldsymbol{r})\psi_\uparrow(\boldsymbol{r}), \quad \Delta_{\boldsymbol{q}} = g_0\int_{\boldsymbol{k}} \psi_{\boldsymbol{q}-\boldsymbol{k}\downarrow}\psi_{\boldsymbol{k}\uparrow} \tag{4}$$

in real or momentum space, respectively [the shorthand notation $\int_{\boldsymbol{k}} \equiv \int d\boldsymbol{k}/(2\pi)^d$]. After a Hubbard-Stratonovich transformation, one obtains the Fermi-Bose action in terms of both fermion and pair degrees of freedom [7,18,19],

$$S = \int d\boldsymbol{r}\int_0^\beta d\tau\Bigg[\sum_\sigma \psi^*_\sigma\left(\partial_\tau - \frac{\nabla^2}{2m} - \mu_\sigma\right)\psi_\sigma - \frac{1}{g_0}|\Delta|^2 - \psi^*_\uparrow\psi^*_\downarrow\Delta - \Delta^*\psi_\downarrow\psi_\uparrow\Bigg], \tag{5}$$

where τ denotes imaginary time (we use units where $\hbar = 1$ from now on). Alternatively, one can start from a two-channel Hamiltonian for fermions and molecules in the broad resonance limit [1].

B. Keldysh technique in equilibrium

The model of coupled fermions and pairs leads to a dressing of both, which is reflected in their renormalized spectra. We will use the Keldysh formulation [20] in equilibrium in order to compute these spectra in real frequency. Although in principle the equilibrium spectra could be obtained from Matsubara Green's functions [21] by analytical continuation, this procedure is mathematically ill-defined and error prone for noisy numerical data. By using the Keldysh formulation, we avoid the need for analytical continuation and obtain reliable spectra directly in real frequency.

The bare retarded fermion Green's function of spin component σ,

$$G^R_{\sigma 0}(\boldsymbol{p},\varepsilon) = \frac{1}{\varepsilon + i0 + \mu_\sigma - \varepsilon_p}, \tag{6}$$

encodes noninteracting particles with dispersion relation $\varepsilon_p = p^2/2m$ and a bare spectral function $A_{\sigma 0}(\boldsymbol{p},\varepsilon) = -(1/\pi)\mathrm{Im}G^R_{\sigma 0}(\boldsymbol{p},\varepsilon) = \delta(\varepsilon + \mu_\sigma - \varepsilon_p)$. In the presence of interactions the bare Green's function turns into the fully dressed Green's function with self-energy $\Sigma^R_\sigma(\boldsymbol{p},\varepsilon)$ via the Dyson equation

$$G^R_\sigma(\boldsymbol{p},\varepsilon) = \frac{1}{\varepsilon + i0 + \mu_\sigma - \varepsilon_p - \Sigma^R_\sigma(\boldsymbol{p},\varepsilon)} = -i\int_0^\infty dt\, e^{i(\varepsilon+i0)t}\langle\{\psi_{\boldsymbol{p}\sigma}(t), \psi^\dagger_{\boldsymbol{p}\sigma}(0)\}\rangle. \tag{7}$$

The bosonic Green's function that represents fermion pairs is analogously given by (with subscript p for pairs)

$$G^R_p(\boldsymbol{q},\omega) = \frac{1}{g_0^{-1} - \Sigma^R_p(\boldsymbol{q},\omega)} = -i\int_0^\infty dt\, e^{i(\omega+i0)t}\langle[\Delta_{\boldsymbol{q}}(t), \Delta^\dagger_{\boldsymbol{q}}(0)]\rangle, \tag{8}$$

with bare coupling g_0 and bosonic self-energy $\Sigma^R_p(\boldsymbol{q},\omega)$.

In our model fermions can scatter off real or virtual pairs and acquire a fermionic self-energy that is given by [20,22] (here $\bar\sigma = -\sigma$ denotes the other fermion species)

$$\Sigma^R_\sigma(\boldsymbol{p},\varepsilon) = -\frac{i}{2}\int_{\boldsymbol{p}',\varepsilon'}\left[G^R_p(\boldsymbol{p}+\boldsymbol{p}', \varepsilon+\varepsilon')G^K_{\bar\sigma}(\boldsymbol{p}',\varepsilon') + G^K_p(\boldsymbol{p}+\boldsymbol{p}', \varepsilon+\varepsilon')G^A_{\bar\sigma}(\boldsymbol{p}',\varepsilon')\right] \tag{9}$$

(see Fig. 1). While the retarded and advanced Green's functions $G^R(\boldsymbol{p},\varepsilon) = [G^A(\boldsymbol{p},\varepsilon)]^*$ represent only the spectrum, the Keldysh components $G^K(\boldsymbol{p},\varepsilon)$ represent both the spectrum and the occupation number with the statistical factor in equilibrium,

$$G^K_\sigma(\boldsymbol{p},\varepsilon) = -i\tanh(\beta\varepsilon/2)A_\sigma(\boldsymbol{p},\varepsilon), \tag{10}$$

$$G^K_p(\boldsymbol{q},\omega) = -i\coth(\beta\omega/2)A_p(\boldsymbol{q},\omega), \tag{11}$$

with full spectral functions $A_\sigma(\boldsymbol{p},\varepsilon) = -(1/\pi)\mathrm{Im}G^R_\sigma(\boldsymbol{p},\varepsilon)$ and $A_p(\boldsymbol{q},\omega) = -(1/\pi)\mathrm{Im}G^R_p(\boldsymbol{q},\omega)$. The occupation factors

can be rewritten in terms of the Fermi and Bose functions as $\tanh(\beta x/2) = 1 - 2f(x)$ with $f(x) = \frac{1}{2}[1 - \tanh(\beta x/2)]$ and as $\coth(\beta x/2) = 1 + 2b(x)$ with $b(x) = \frac{1}{2}[\coth(\beta x/2) - 1]$. In this way, the retarded fermionic self-energy is expressed as

$$\Sigma^R_\sigma(\boldsymbol{p},\varepsilon) = \int_{\boldsymbol{p}',\varepsilon'} \big[G^R_p(\boldsymbol{p}+\boldsymbol{p}',\varepsilon+\varepsilon')f(\varepsilon')A_{\bar\sigma}(\boldsymbol{p}',\varepsilon') - b(\varepsilon+\varepsilon')A_p(\boldsymbol{p}+\boldsymbol{p}',\varepsilon+\varepsilon')G^A_{\bar\sigma}(\boldsymbol{p}',\varepsilon')\big], \quad (12)$$

where a contribution independent of occupation vanishes by analyticity. For the imaginary part of the self-energy, the occupation factors are combined with a product of spectral functions as

$$\mathrm{Im}\Sigma^R_\sigma(\boldsymbol{p},\varepsilon) = -\pi \int_{\boldsymbol{p}',\varepsilon'} [f(\varepsilon') + b(\varepsilon+\varepsilon')] \times A_p(\boldsymbol{p}+\boldsymbol{p}',\varepsilon+\varepsilon')A_{\bar\sigma}(\boldsymbol{p}',\varepsilon'). \quad (13)$$

Once the imaginary part has been computed, the real part can be obtained by the Kramers-Kronig relation

$$\mathrm{Re}\Sigma^R(\boldsymbol{p},\varepsilon) = \int \frac{d\varepsilon'}{\pi}\mathcal{P}\frac{\mathrm{Im}\Sigma^R(\boldsymbol{p},\varepsilon')}{\varepsilon'-\varepsilon}, \quad (14)$$

which involves an integral over the principal value $\mathcal{P}$.

The bosonic self-energy in turn arises from dissociation of a pair into individual fermions and is computed as the particle-particle bubble diagram (see Fig. 1),

$$\begin{aligned}\Sigma^R_p(\boldsymbol{q},\omega) &= \frac{i}{2}\int_{\boldsymbol{p},\varepsilon} [G^R_\uparrow(\boldsymbol{q}-\boldsymbol{p},\omega-\varepsilon)G^K_\downarrow(\boldsymbol{p},\varepsilon) + G^K_\uparrow(\boldsymbol{q}-\boldsymbol{p},\omega-\varepsilon)G^R_\downarrow(\boldsymbol{p},\varepsilon)] \\ &= \int_{\boldsymbol{p},\varepsilon} \big\{G^R_\uparrow(\boldsymbol{q}-\boldsymbol{p},\omega-\varepsilon)\big[\tfrac{1}{2} - f(\varepsilon)\big]A_\downarrow(\boldsymbol{p},\varepsilon) + \big[\tfrac{1}{2} - f(\omega-\varepsilon)\big]A_\uparrow(\boldsymbol{q}-\boldsymbol{p},\omega-\varepsilon)G^R_\downarrow(\boldsymbol{p},\varepsilon)\big\}. \end{aligned} \quad (15)$$

Both terms can be combined after a change of variables to yield

$$\mathrm{Im}\Sigma^R_p(\boldsymbol{q},\omega) = -\pi\int_{\boldsymbol{p},\varepsilon}[1-2f(\varepsilon)]A_\uparrow(\boldsymbol{p},\varepsilon) \times A_\downarrow(\boldsymbol{q}-\boldsymbol{p},\omega-\varepsilon). \quad (16)$$

Causality implies that the imaginary part of the fermionic Green's function is always negative, $\mathrm{Im}G^R_\sigma(\boldsymbol{p},\varepsilon) < 0\,\forall\,\varepsilon$, while the imaginary part of the bosonic Green's function changes sign at $\omega = 0$, $\mathrm{Im}G^R_p(\boldsymbol{q},\omega)\mathrm{sgn}(\omega) < 0$. The same holds for the sign of the imaginary parts of the fermionic and bosonic self-energies, which follows from their definitions (12) and (16). Equations (7), (8), (12), and (16) form a closed set of coupled integral equations for the fermion and pair Green's functions. This particular set of equations corresponds to the self-consistent Luttinger-Ward approach [12,23,24]. In the following we present a method for their numerical solution in real frequency.

The Keldysh technique introduced so far applies to general polarized Fermi gas with $\mu_\uparrow \neq \mu_\downarrow$. In this work we will start by presenting the solution for the case of a balanced (unpolarized) gas with $\mu_\uparrow = \mu_\downarrow = \mu$ and $G_\uparrow = G_\downarrow \equiv G_\sigma$.

C. Quantum virial expansion

Since we are interested in the strongly correlated Fermi gas at large scattering length $|a|$, the interaction strength is not a good expansion parameter. Instead, in the high-temperature normal state one can perform a quantum virial expansion in the fermionic fugacity

$$z = \exp(\beta\mu) \quad (17)$$

as the small parameter, where $\beta = 1/k_BT$ denotes the inverse temperature and we work henceforth in units where $k_B \equiv 1$. In the high-temperature virial expansion we can already identify spectral features that will be important reference points in the discussion of the low-temperature spectra below. When pairing is important the pair fugacity

$$z_p = \exp(\beta\mu_p) = \exp[\beta(2\mu + E_b)] = z^2e^{\beta E_b} \quad (18)$$

controls the strength of pair contributions with pair chemical potential $\mu_p = 2\mu + E_b$. One can distinguish the fermion-dominated regime $z_p < z$ from the pair-dominated regime $z_p > z$ [25]. In the expressions for the self-energy (12) and (16), the Fermi function is expanded for small fugacity as $f(x-\mu) = ze^{-\beta x} + O(z^2)$ and the Bose function as $b(x-\mu_p) = z_pe^{-\beta x} + O(z_p^2) = z^2e^{\beta E_b}e^{-\beta x} + O(z^4)$.

To zeroth order in fugacity, i.e., in vacuum, the fermion self-energy vanishes and the bosonic self-energy is known analytically as

$$\begin{aligned}\Sigma^R_{p0}(\boldsymbol{q},\omega) &= \int_{\boldsymbol{p}}^{\Lambda} G^R_{\sigma 0}(\boldsymbol{q}-\boldsymbol{p},\omega+\mu-\varepsilon_p) \\ &= \frac{m}{4\pi}\sqrt{-m(\omega+2\mu-\tfrac{1}{2}\varepsilon_q+i0)} - \frac{m\Lambda}{2\pi^2}\end{aligned} \quad (19)$$

for large cutoff $\Lambda \to \infty$. The cutoff term in the definition of the bare coupling g_0 (2) cancels that in the self-energy to yield the cutoff-independent pair Green's function [6]

$$G^R_{p0}(\boldsymbol{q},\omega) = \frac{4\pi/m}{a^{-1} - \sqrt{-m\big(\omega+2\mu-\frac{1}{2}\varepsilon_q+i0\big)}}. \quad (20)$$

The corresponding pair spectral function reads

$$A_{p0}(\boldsymbol{q},\omega) = \frac{4\pi}{m^{3/2}}\left(2\sqrt{E_b}\delta(s_p+E_b)\Theta(a) + \frac{1}{\pi}\frac{\sqrt{s_p}\Theta(s_p)}{s_p+1/ma^2}\right)_{s_p=\omega+2\mu-\varepsilon_q/2} \quad (21)$$

in terms of the pair spectral parameter $s_p = \omega + 2\mu - \varepsilon_q/2$, which measures the energy from the onset of the scattering continuum at $s_p = 0$. The pair spectrum exhibits a scattering continuum for $s_p > 0$ from the square root branch cut, and for positive $a > 0$ there is additionally the pair bound state at $s_p = -E_b$ with pair dispersion $\omega_q = q^2/2M$ at twice the fermion mass $M = 2m$. Note that the pair spectrum in vacuum is still Galilean invariant, i.e., it depends only on the combination s_p and not on ω or $\boldsymbol{q}$ separately. This will no longer be the case at finite density, as we will see below.

At finite density the Fermi distribution has to be included in the bosonic self-energy even when using bare fermion propagators $G_{\sigma 0}$, and the bosonic self-energy for bare fermions reads

$$\Sigma_p^{(1)R}(\boldsymbol{q},\omega) = \int_{\boldsymbol{p}} [1-2f(\varepsilon_p-\mu)] G^R_{\sigma 0}(\boldsymbol{q}-\boldsymbol{p},\omega+\mu-\varepsilon_p), \tag{22}$$

$$\mathrm{Im}\,\Sigma_p^{(1)R}(\boldsymbol{q},\omega) = \frac{m}{4\pi}\left(-\sqrt{m s_p} + \frac{2mT}{q}\ln\frac{1-f(\omega/2+\sqrt{\varepsilon_q s_p/2})}{1-f(\omega/2-\sqrt{\varepsilon_q s_p/2})}\right)\Theta(s_p). \tag{23}$$

While the real part is not known analytically, it is easily obtained by numerical Kramers-Kronig transformation (14) since the finite-temperature correction (second term) decays exponentially for large frequency $\omega \gg T$. In the limit $q \to 0$ the imaginary part simplifies to $\mathrm{Im}\,\Sigma_p^{(1)R}(\boldsymbol{q}=0,\omega) = -(m/4\pi)\sqrt{m s_p}\tanh(\beta\omega/4)\Theta(s_p)$. Both in this expression and in Eq. (23) the sign of the imaginary part changes at $\omega = 0$ as required by causality. As is clear from Eq. (23), the self-energy at nonzero density depends no longer only on s_p but also on ω or q separately and the pair propagator in the medium does not have a Galilean invariant form.

As the density is further increased the attractive Fermi gas undergoes a phase transition into a superfluid state. This occurs when pairs can be excited at zero momentum $q = 0$ and zero energy $\omega = 0$, as given by the Thouless criterion $[G_p^R(\boldsymbol{q}=0,\omega=0)]^{-1} = 0$ [6]. With bare fermions this is equivalent to $a^{-1} = (2/\pi)\int_0^\infty ds\,\frac{\sqrt{ms}}{s-2\mu} f(s/2-\mu)$. At weak coupling $a \to 0^-$ it yields the critical temperature $(\beta\mu)_c^{-1} = (8e^{\gamma-2}/\pi)\exp(\pi/2k_F a)$, but at stronger coupling no analytical expression is known. At unitarity, the non-self-consistent calculation with bare propagators yields $(\beta\mu)_c \approx 1.5$, while experiment [10] and self-consistent Luttinger-Ward theory [12] yield a value of $(\beta\mu)_c \approx 2.5$, corresponding to $T_c/T_F \approx 0.16$.

III. SELF-CONSISTENT SOLUTION IN REAL FREQUENCY

At low temperatures in the normal state $T > T_c$, one can reach $z \gtrsim 1$ and the virial expansion does not converge. Instead, we will now present a real-frequency solver for the coupled integral equations (7), (8), (12), and (16). In continuous time and space, one can choose a grid of frequencies ε_i to sample the full domain $-\infty < \varepsilon < \infty$ and a grid of radial momenta p_j for $0 \leqslant p < \infty$. The challenge of a straightforward numerical solution is that the spectral function $A(\boldsymbol{p},\varepsilon)$ can have very narrow δ peaks at large frequencies or momenta even in a strongly correlated system, making it difficult to resolve these peaks on a grid. Such narrow peaks, however, often arise as simple poles where the denominator has a zero crossing and is well described by a linear approximation of the denominator between grid points. Hence, we propose an inverse integrator that interpolates the denominator of the Green's function. Such an approximation becomes accurate if the self-energy $\Sigma(\boldsymbol{p},\varepsilon)$ varies only slowly with $\boldsymbol{p}$ and ε. Using a linear interpolation of the self-energy between grid points, the value of the frequency or momentum integral of the Green's function can be computed analytically, depending on the value of Σ on the adjacent grid points. Explicitly, we obtain, with $x = (p^2-p_j^2)/(p_{j+1}^2-p_j^2)$,

$$\int_{p_j}^{p_{j+1}} dp\, p\, G(p,\varepsilon) = \frac{p_{j+1}^2-p_j^2}{2}\int_0^1 \frac{dx}{a+bx} = \frac{p_{j+1}^2-p_j^2}{2}\frac{\ln(G_{j+1}^{-1}G_j)}{G_{j+1}^{-1}-G_j^{-1}}, \tag{24}$$

where $a = G^{-1}(p_j,\varepsilon)$ and $a+b = G^{-1}(p_{j+1},\varepsilon)$ are given in terms of the self-energy at the grid points. An analogous formula applies for integration over frequency ε between grid points. This integral is exact for noninteracting particles and it is a good approximation for slowly varying Σ; note that there is no need for Σ to be small and so the validity extends to strong coupling beyond the virial expansion. The numerical results below show that Σ changes in frequency roughly on the scale of the temperature T and in momentum over $\sqrt{2mT}$, so in practice it is sufficient to use a frequency grid $\varepsilon = -100T, \ldots, 100T$ with equidistant spacing $\Delta\varepsilon = 0.5T$ and a momentum grid $p = 0, \ldots, 10\sqrt{2mT}$ with spacing $\Delta p = 0.2\sqrt{2mT}$. For the lowest temperatures in our study, $T/T_F = 0.16$, this corresponds to a self-energy grid spacing $\Delta\varepsilon = 0.08\varepsilon_F$ and $\Delta p = 0.08k_F$.

The explicit formula for the one-loop renormalization of the fermion and pair spectra, which has the form of a convolution integral (13), can be written as

$$\mathrm{Im}\,\Sigma_\sigma^R(\boldsymbol{p},\varepsilon) = -\pi\int_{-\infty}^{\infty} d\varepsilon'\,[f(\varepsilon')+b(\varepsilon+\varepsilon')] \times \frac{1}{4\pi^2 p}\int_0^\infty dq\, q\, A_p(q,\varepsilon+\varepsilon') \times \int_{|p-q|}^{p+q} dp'\, p' A_{\bar\sigma}(p',\varepsilon'). \tag{25}$$

Here, the momentum integral has been expressed as an integral over the bosonic radial momentum q and the fermionic radial momentum p', weighted by $\Theta(|p-q| < p' < p+q)/(4\pi^2 p)$. The principal function of the p' integral is computed first using formula (24), which takes $\mathcal{O}(N)$ time for N momentum-frequency grid points. While the spectral function can have δ peaks, its principal function has at most steps of unit height, such that the error from a discretization Δp of the momentum integral is at most $\mathcal{O}(\Delta p)$. The subsequent q,ε' integration for every p,ε takes $\mathcal{O}(N^2)$ time for the complete self-energy, which is the most time-intensive computational step. Finally, the Kramers-Kronig transformation (14) is employed to obtain the real part of the self-energy; this ensures exact analyticity of the self-energy even if $\mathrm{Im}\,\Sigma$ is computed approximately.

At high temperature or weak coupling the fermionic self-energy follows approximately the result of perturbation theory, which has a square-root nonanalyticity, but the absolute magnitude of the self-energy is small. Conversely, at low temperature and strong coupling the self-energy is much larger (of order T) but at the same time the functional form

is smoothed by an imaginary part of order T. As a result, the slope of the fermionic self-energy with respect to energy, $|d\Sigma_\sigma/d\varepsilon|$, is bounded as $\mathcal{O}(1)$ for all energies and momenta. This is confirmed numerically for the self-energies shown in Fig. 3 below. Hence, the maximum discretization error in Σ_σ is bounded as $\mathcal{O}(\Delta\varepsilon)$ and by refining the grid spacing the discretization error can be systematically reduced.

The frequency integral is weighted by the fermionic and bosonic occupation factors. While the fermionic occupation is always positive and smooth, weighting by the bosonic occupation requires care as $b(\omega) \simeq \frac{T}{\omega} - \frac{1}{2}$ for $|\omega| \ll T$. In the Keldysh formulation, however, the Bose function appears always in combination with a bosonic spectral function $A_p(\omega)$, which changes sign at $\omega = 0$ and scales linearly in ω for $|\omega| \ll T$. The product of bosonic spectrum and occupation, therefore, is continuous and well-behaved near $\omega = 0$. One can easily check that also the combination $f(\varepsilon') + b(\varepsilon + \varepsilon')$ in Eq. (25) changes sign when $\varepsilon + \varepsilon' = 0$ such that the $\mathrm{Im}\,\Sigma^R_\sigma(p, \varepsilon) < 0\ \forall\varepsilon$, as required by causality.

As we will see below, the fermionic self-energy $\mathrm{Im}\,\Sigma_\sigma$ scales asymptotically as $\varepsilon^{-1/2}$ for large frequencies. This tail is important in the Kramers-Kronig transformation in order to accurately obtain the real part $\mathrm{Re}\,\Sigma_\sigma$ near the Fermi surface, which determines the shift of the spectral lines. We include the asymptotic tail beyond the maximum grid frequency analytically in the Kramers-Kronig transformation. In the convolution integral, instead, the high-frequency parts are suppressed by the Fermi and Bose distributions and give only a small contribution.

Analogously, the bosonic self-energy is computed explicitly as

$$\begin{aligned}\mathrm{Im}\,\Sigma^R_p(\boldsymbol{q}, \omega) = &-\pi \int_{-\infty}^{\infty} d\varepsilon [1 - 2f(\varepsilon)] \\ &\times \frac{1}{4\pi^2 q} \int_0^\infty dp\, p A_\uparrow(p, \omega - \varepsilon) \\ &\times \int_{|p-q|}^{p+q} dp'\, p' A_\downarrow(p', \varepsilon). \end{aligned} \tag{26}$$

The set of self-consistent integral equations can be solved by iteration. As initial condition we choose bare fermions with $\Sigma^{(0)}_\sigma(p, \varepsilon) \equiv -i0$ (in practice we use $-10^{-8} iT$). Each iteration consists of two steps.

Step 1. Compute the new pair self-energy from Eq. (26) and numerical Kramers-Kronig transformation (14) for the real part. The convolution integral Σ_p is evaluated using the fermionic self-energies $\Sigma_{\uparrow,\downarrow}$ of the i-th iteration

$$\Sigma^{(i+1)}_p = \Sigma_p[\Sigma^{(i)}_\uparrow, \Sigma^{(i)}_\downarrow]. \tag{27}$$

In the first iteration for $\Sigma^{(1)}_p$ we use the analytical formula (19) for accuracy.

Step 2. Compute the new fermion self-energy from Eqs. (25) and (14),

$$\Sigma^{(i+1)}_\sigma = \alpha \Sigma_\sigma\big[\Sigma^{(i+1)}_p, \Sigma^{(i)}_{\bar\sigma}\big] + (1 - \alpha)\Sigma^{(i)}_\sigma. \tag{28}$$

A convergence enhancement factor $0 < \alpha \leqslant 1$ can accelerate convergence, and the converged result for $\alpha < 1$ is the same self-consistent solution as for $\alpha = 1$.

Convergence is typically reached after a dozen steps (a bit slower near T_c); we denote the converged self-consistent solution by $\Sigma^{(\infty)}$ and $G^{(\infty)}$. In practice, convergence is fastest if one uses the fully converged solution for a given parameter value μ as the initial condition for a new calculation at a neighboring parameter value $\mu + \delta\mu$.

IV. LUTTINGER-WARD SPECTRA

The procedure in Sec. III produces self-consistent solutions for single-particle and pair Green's functions G^R_σ and G^R_p in real frequency. A crucial feature of this Luttinger-Ward approach is that the results are thermodynamically consistent [19,23]: The density, for instance, is obtained identically either from the grand potential by a thermodynamic derivative or by loop integration over the single-particle Green's function as

$$n_\sigma = \int_{-\infty}^{\infty} d\varepsilon\, f(\varepsilon) g_\sigma(\varepsilon), \quad g_\sigma(\varepsilon) = \int \frac{d^3p}{(2\pi)^3} A_\sigma(p, \varepsilon), \tag{29}$$

$$\mathcal{C} = m^2 \int_{-\infty}^{\infty} d\omega\, b(\omega) g_p(\omega), \quad g_p(\omega) = \int \frac{d^3q}{(2\pi)^3} A_p(q, \omega), \tag{30}$$

where we have defined the single-component fermion density n_σ and density of states $g_\sigma(\varepsilon)$. In (30) the local pair density, or contact $\mathcal{C}$, is defined via an integral over the pair density of states $g_p(\omega)$, with an additional mass factor m^2 by convention. The thermodynamic results for the fermion density and the contact (pair) density agree with previous self-consistent Luttinger-Ward computations in imaginary frequency [12]. In order to showcase our method, we choose applications to two distinct physical regimes of the strongly correlated Fermi gas: (i) the unitary regime at the scattering resonance ($a^{-1} = 0$) where spectra are dominated by many-body BCS-type pairing ($z_p \leqslant z^2$) and (ii) the Bose-Einstein condensate (BEC) regime [$(k_F a)^{-1} \simeq 1$] where two-body binding has a substantial effect on many-body properties ($z_p \gg z^2$).

A. Particle and pair spectra at unitarity

Figures 2 and 3 show the resulting self-energies and spectra for both fermions and pairs in the unitary regime ($\beta E_b = 0$). First Fig. 2 presents the line spectra for the frequency dependence at vanishing momentum, which already exhibits many qualitative features of the full spectrum in Fig. 3. For $\beta\mu = 1$ in the quantum degenerate regime, corresponding to $T/T_F \approx 0.3$, the high-temperature virial expansion (A3) to first order in fugacity predicts a single narrow peak in the imaginary part of the self-energy [brown dashed line in Fig. 2(a)]. The first iteration of the Luttinger-Ward scheme, computed with bare fermions, includes contributions to arbitrary order in fugacity and displays already a much broader single peak for this large value of fugacity, $z = e^1$. The full self-consistent solution instead shows a qualitatively different behavior with a two-peak structure, which becomes more pronounced as the chemical potential is increased to $\beta\mu = 1.5, 2.0, 2.5$, corresponding to temperatures approaching $T/T_F \simeq 0.16$ just above T_c (blue curve). Correspondingly, the fermion spectrum in Fig. 2(b)

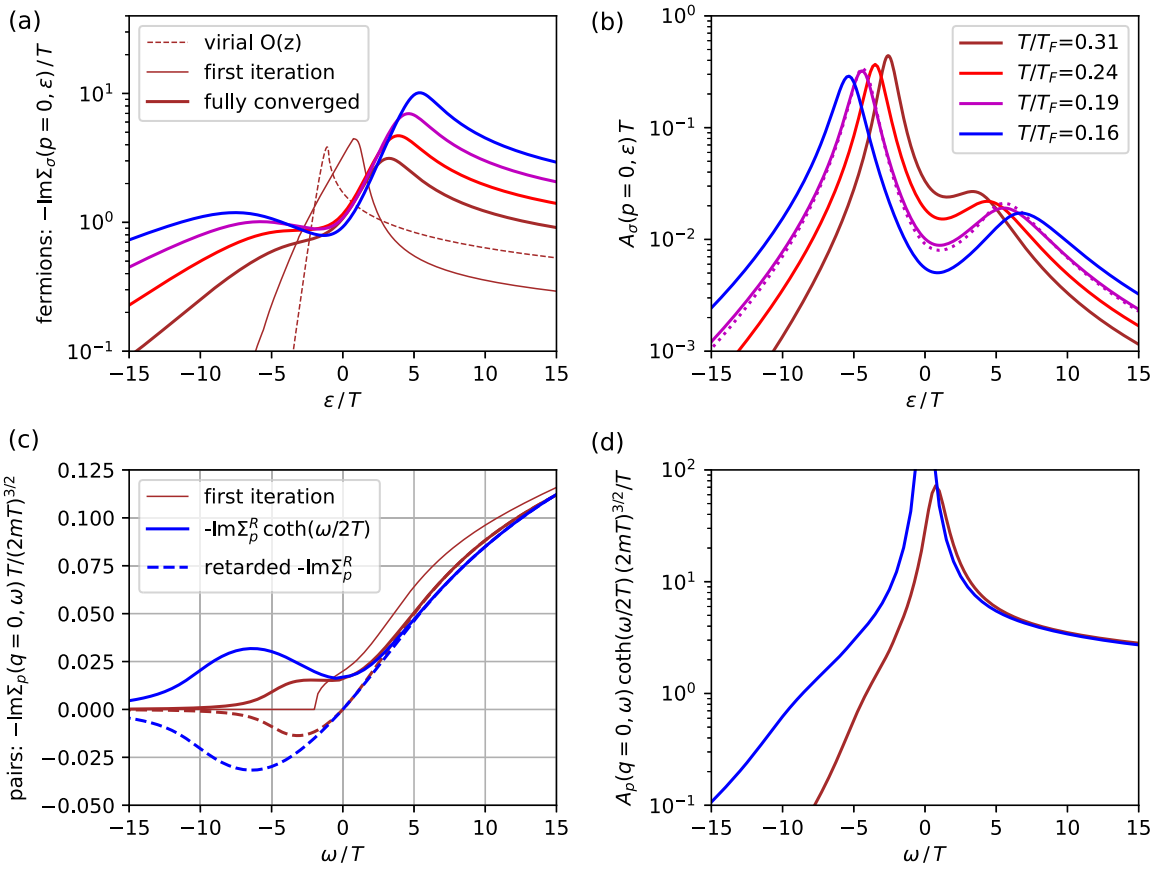

FIG. 2. Line spectra of fermions and pairs at unitarity: real frequency dependence at zero momentum. Temperatures are in the normal state approaching T_c: $T/T_F = 0.31$ ($\beta\mu = 1.0$, brown), $T/T_F = 0.24$ ($\beta\mu = 1.5$, red), $T/T_F = 0.19$ ($\beta\mu = 2.0$, magenta), and $T/T_F = 0.16$ ($\beta\mu = 2.5$, blue). (a) The fermion self-energy shows a single peak in the virial expansion (dashed line) and a renormalized single peak in the first LW iteration $\Sigma_\sigma^{(1)}$ (thin line); instead, the fully converged self-energy $\Sigma_\sigma^{(\infty)}$ (thick line) develops a two-peak structure which grows more prominent as the temperature is lowered. (b) The fermion spectrum shows a two-peak structure as a precursor to the Bogoliubov spectrum. The comparison with spectral data of Ref. [26] (dotted line) shows good agreement. (c) The pair self-energy has a zero crossing at $\omega = 0$ by causality (dashed line); the spectral weight at negative frequencies is enhanced at lower temperature. The Keldysh component $-\mathrm{Im}\Sigma_p(q = 0, \omega)\coth(\omega/2T)$ (solid line) remains positive at all frequencies and regular around $\omega = 0$. (d) The pair spectrum has a single asymmetric peak near threshold that becomes broader and more pronounced at lower temperature.

develops a two-peak structure as a precursor to the Bogoliubov spectrum as the temperature is lowered.

The imaginary part of the pair self-energy in Fig. 2(c) arises from dissociation of pairs into individual fermions; it has a square-root branch cut representing the scattering continuum for large frequencies. As a bosonic function it must change sign at $\omega = 0$ (dashed curves). When weighted with the Bose factor, $-\mathrm{Im}\Sigma_p(\omega)\coth(\omega/2T) > 0$ is regular at $\omega = 0$ and positive for all frequencies (solid curves). Note that the fully converged self-consistent solution (thick lines) contains substantially more spectral weight at smaller frequencies $\omega < 0$ than the first iteration (thin line), in particular at lower temperature (blue curves). Finally, the pair spectral function in Fig. 2(d) weighted with the Bose factor [the Keldysh component (10)] is positive and exhibits a single large peak for the onset of the scattering continuum, which decays for large frequencies as $\omega^{-1/2}$. This slow decay in turn determines also the decay of the fermionic self-energy as $\varepsilon^{-1/2}$ for large frequencies.

The full spectra at $T = 0.16T_F$ slightly above T_c are shown in Fig. 3. The fermion self-energy has a broad upward branch starting at $\varepsilon \sim \varepsilon_{\boldsymbol{p}}/2$, which arises from combining with another low-momentum fermion into a pair state (molecule-hole continuum), and a steeper downward branch $\varepsilon \sim -\varepsilon_{\boldsymbol{p}}$, which arises from combining with another fermion into a low-momentum pair. The imaginary part of the self-energy determines the decay rate (inverse lifetime) of the corresponding fermion states, which near T_c is substantial (comparable to ε_F). These spectral features are reflected in the fermion spectral function Fig. 3(b), which shows a band splitting around the Fermi level $\varepsilon = 0$ and the appearance of Bogoliubov shadow bands already above T_c. Note that the fermionic self-energy and spectral function clearly do not follow a single-parameter scaling in terms of the spectral parameter $s = \varepsilon + \mu - \varepsilon_{\boldsymbol{p}}$ alone.

The pair self-energy in Fig. 3(c) clearly exhibits the scattering continuum for $\omega \gtrsim \varepsilon_{\boldsymbol{q}}/2 - 2\mu$. In the self-consistent solution, where a pair can dissociate into dressed fermion

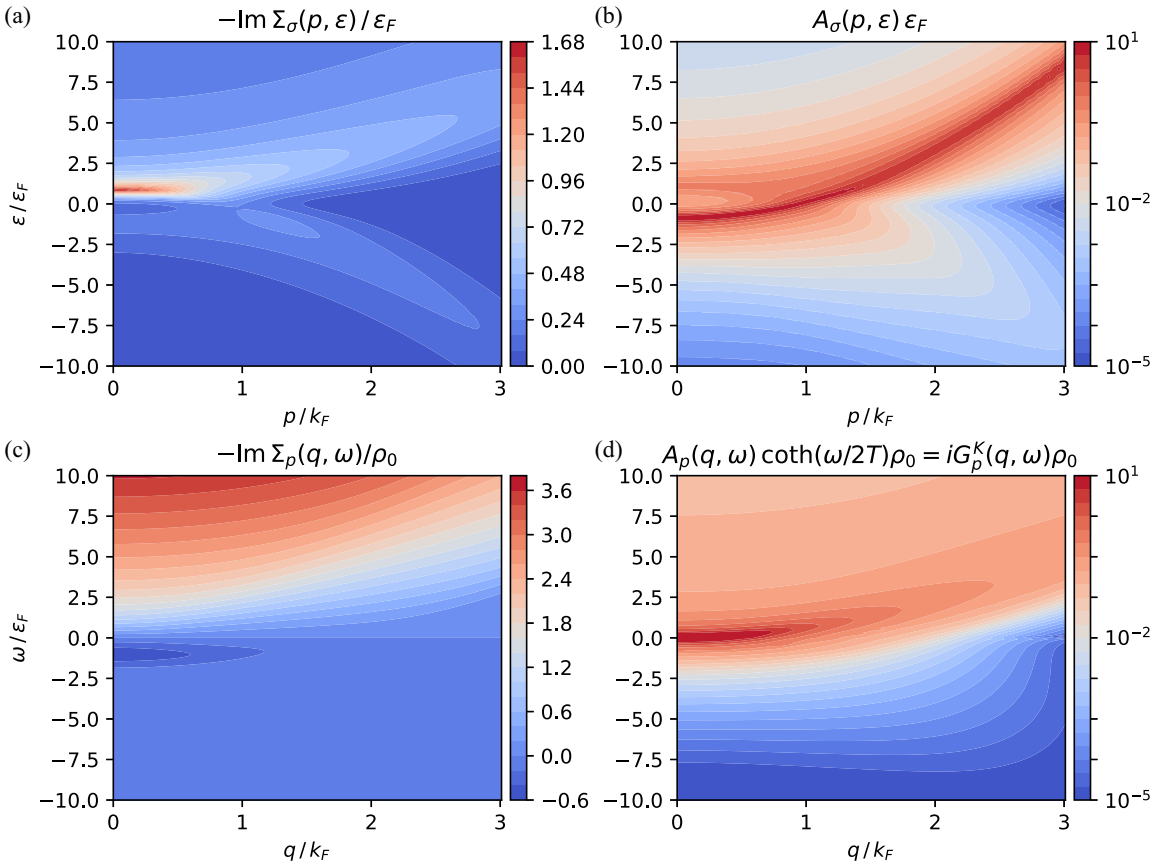

FIG. 3. Luttinger-Ward self-energies and spectral functions at unitarity $1/a = 0$ and temperature $T/T_F = 0.16$ ($\beta\mu = 2.5$). (a) Fermion self-energy. (b) The fermion spectral function shows a band splitting around the Fermi level $\varepsilon = 0$ and a slight suppression of spectral weight also near k_F. (c) Pair self-energy. (d) The pair spectral function weighted by the Bose factor (Keldysh component) is positive and strongly peaked at the threshold of the scattering continuum. Pair functions are given in units of the zero-temperature density of states $\rho_0 = g_\sigma^{(0)} = mk_F/2\pi^2$.

states, the substantial broadening of the fermions shifts the threshold of the scattering continuum to lower frequency with respect to the non-self-consistent solution. Finally, the full pair spectrum in Fig. 3(d) shows the clear threshold of the scattering continuum as well as an additional downward branch that arises from the dressed fermions.

B. Particle and pair spectra in the BEC regime

In the BEC regime the fermion line spectra in Figs. 4 and 5 show many of the same qualitative features, such as upward and downward branches, as in the unitary regime; however, the splitting between the two branches in the fermionic spectrum is now much larger, approximately equal to $2|\mu| > 0$, and grows with momentum, as in the strong-binding limit of the BCS dispersion relation [27]. The pair self-energy is dominated by the scattering continuum but has again significant weight at negative frequency that arises from the downward branch of the dressed fermions. Finally, the pair spectral function (Keldysh component) in Figs. 4(d) and 5(d) exhibits a three-peak structure: The large bound-state peak near $\omega = 0$ becomes broader for lower temperature, the scattering continuum is separated from the bound state by a gap comparable to the binding energy E_b, and in addition there is a downward branch at negative frequencies.

The fermion dispersion exhibits qualitative differences between the unitary regime, where it resembles the BCS-type dispersion relation with minimum gap at nonzero wave vector $k_* \approx k_F$, and the BEC regime, where the gap is present at all k and reaches a minimum at $k = 0$. This qualitative change between the two regimes is also apparent in the density of states (DOS). While at unitarity the density of states is only slightly suppressed near the Fermi level $\varepsilon = 0$ above T_c [cf. Fig. 3(b)], in the BEC regime the gap is clearly developed already in the normal state (cf. Fig. 6), but instead it becomes narrower (in units of ε_F) toward lower temperature.

V. DISCUSSION

The real-frequency solver presented in this work circumvents the long-standing problem of analytical continuation by computing a self-consistent solution directly in the Keldysh spectral representation. This gives access to the dynamical properties of single particles, which agree with previous results where available [28]. At strong coupling they show a substantial renormalization of spectra compared to the virial expansion, and in particular the self-consistent algorithm

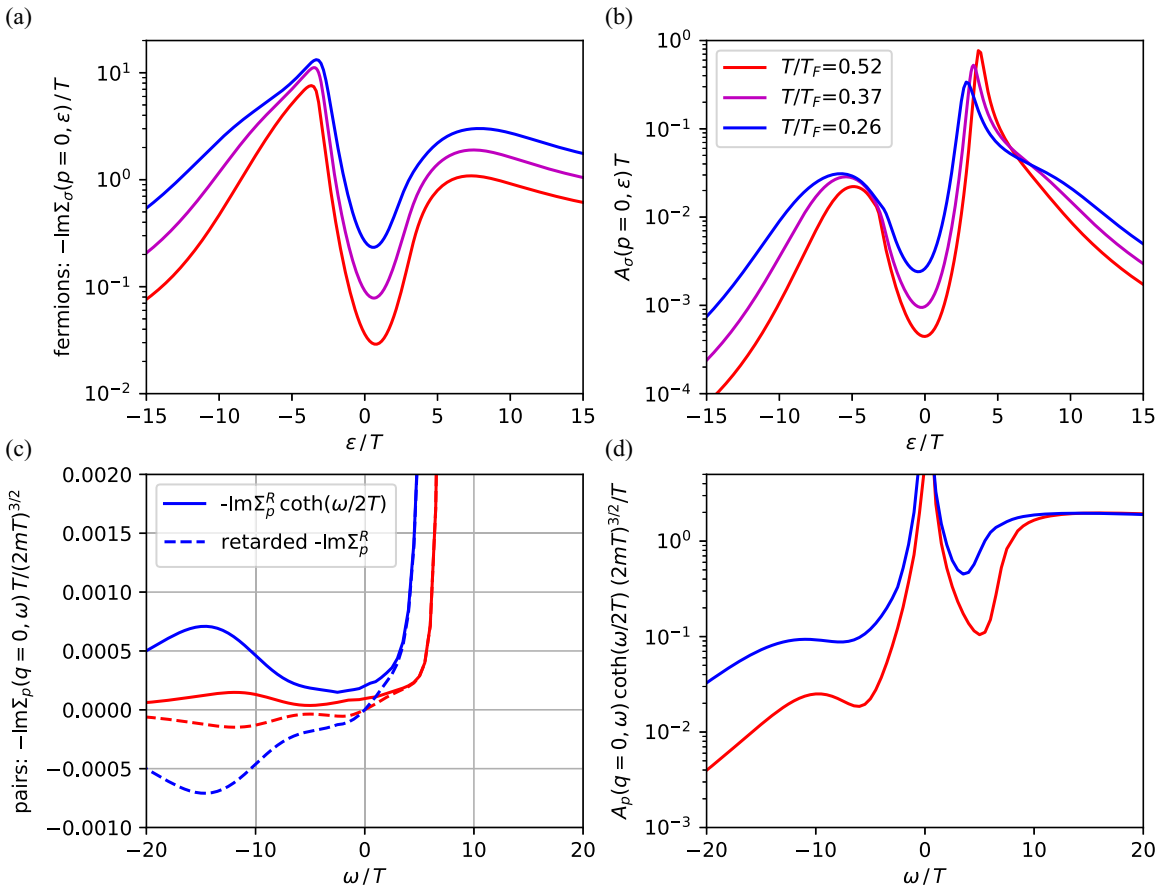

FIG. 4. Line spectra of fermions and pairs in the BEC regime ($\beta E_b = 8$): real frequency dependence at zero momentum. Temperatures are in the normal state approaching T_c: $T/T_F = 0.52$ ($\beta\mu = -4$, red), $T/T_F = 0.37$ ($\beta\mu = -3.75$, magenta), and $T/T_F = 0.26$ ($\beta\mu = -3.5$, blue). (a) The fermion self-energy shows a much more pronounced two-peak structure than at unitarity. (b) The fermion spectrum similarly shows a two-peak structure as a precursor to the Bogoliubov spectrum. (c) The pair self-energy has a zero crossing at $\omega = 0$ by causality (dashed line); the spectral weight at negative frequencies is enhanced at lower temperature. The Keldysh component $-\mathrm{Im}\Sigma_p(q=0,\omega)\coth(\omega/2T)$ (solid) remains positive at all frequencies and regular around $\omega = 0$. (d) The pair spectrum has a triple-peak structure: a large bound-state peak near $\omega = 0$, the scattering continuum for positive ω separated by a gap from the bound state, and a small peak at negative frequency.

allows us to access the low-temperature regime $\beta\mu > 1.5$ at unitarity, which is unattainable in bare perturbation theory. The self-consistent solution in the Luttinger-Ward framework ensures thermodynamic consistency and the exact fulfillment of Tan relations, as well as scale invariance in the unitary case even for approximate solutions [19]. In particular, existing thermodynamic results [e.g., $\mu(n)$] obtained in imaginary frequency can be used as input for the real-frequency computation. On the technical level, in the Keldysh formulation the divergence of the bosonic occupation at zero frequency is compensated by the smallness of the bosonic spectral function to yield a well-defined frequency integral, but it can still have sharp peaks from long-lived excitations. Our algorithm treats these efficiently by interpolation of the self-energy, which is a slowly varying function between grid points. The accuracy of the spectra is confirmed by comparing with results for finer grids ($\Delta\varepsilon = 0.25T$) and with the spectral data of Ref. [26]. By construction, the resulting Green's functions satisfy the requirements of analyticity and causality. The Luttinger-Ward spectra with their subtle three-peak structure (Fig. 4) can serve as a benchmark and as a prior for the numerical reconstruction of imaginary-time quantum Monte Carlo data.

The real-frequency solver can immediately be applied to imbalanced (polarized) Fermi gases with $\mu_\uparrow \neq \mu_\downarrow$; in fact, the equations in Sec. II are already written for this general case. This will allow one to extend self-consistent ground-state polaron spectra [29] to finite temperature. Furthermore, the self-consistent thermodynamics in the symmetry-broken superfluid state has been found in the balanced [12] and imbalanced Fermi gas [14], and it will be worthwhile to extend the real-frequency solver to this case in order to obtain the corresponding excitation spectra. Another important extension will be to the two-dimensional Fermi gas [30], which always admits a pair bound state with $E_b > 0$ and is therefore covered by our algorithm for the BEC regime; this will allow for a self-consistent computation of pairing spectra [27,31] and the dynamical quantum scale anomaly [32,33].

Another very interesting extension is to compute dynamical correlation and response functions, which define, e.g., transport coefficients such as shear viscosity [34,35], bulk viscosity [25,36–39], thermal conductivity [40,41],

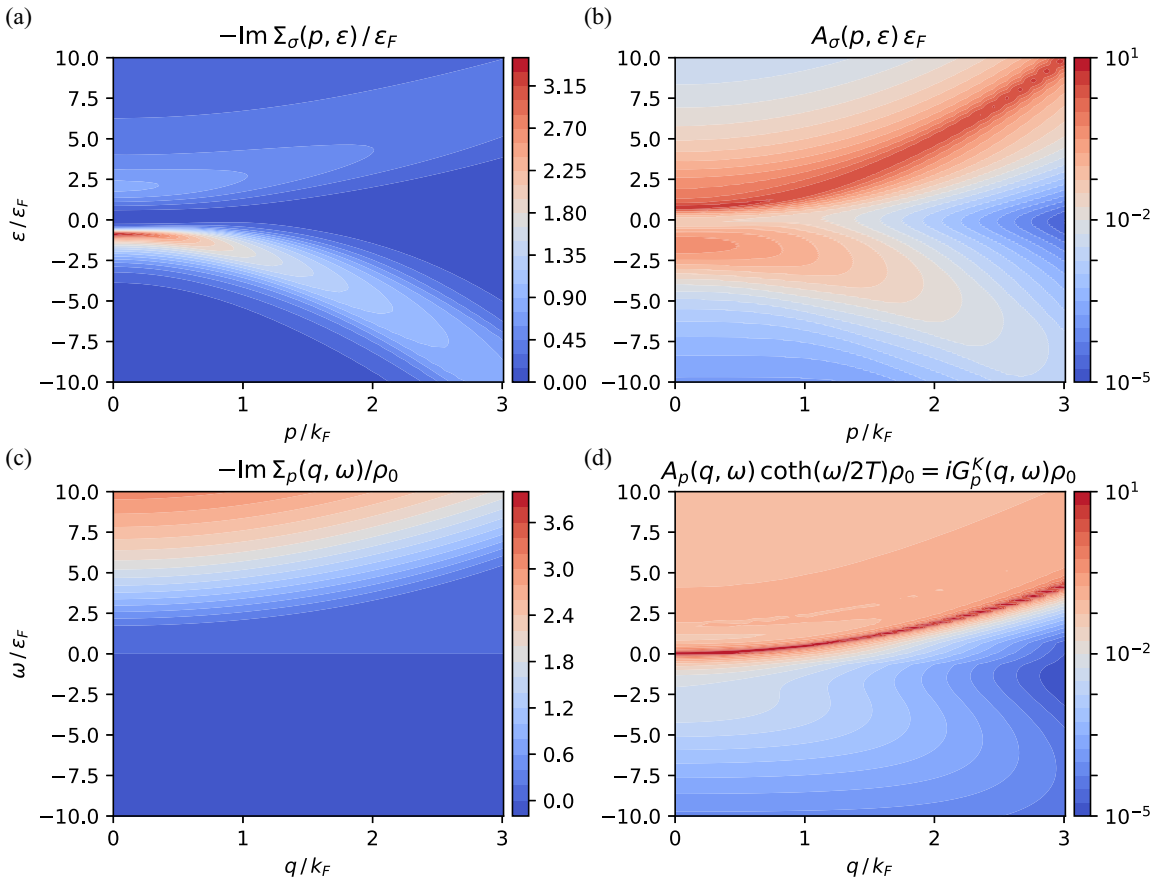

FIG. 5. Luttinger-Ward self-energies and spectra in the BEC regime $1/k_F a = 1$ at $T/T_F = 0.26$ ($\beta\mu = -3.5$) slightly above T_c. (a) The fermion self-energy $\Sigma_\sigma(p,\varepsilon)$ shows two branches and fermions scatter most strongly on the lower branch. (b) The fermion spectral function $A_\sigma(p,\varepsilon)$ shows a clear gap between the two branches around the Fermi level $\varepsilon = 0$ and has most spectral weight concentrated on the upper branch. (c) The pair self-energy $\Sigma_p(q,\omega)$ shows the two-particle scattering continuum. (d) The weighted pair spectral function $A_p(q,\omega)\coth(\omega/2T) = iG_p^K$ (the pair Keldysh function) shows a strong bound-state branch separated by the binding energy $E_b = 2E_F$ from the pair continuum, as well as a weak branch bending down.

and spin diffusivity [42,43]. As the frequency-dependent transport coefficients depend on the slope in frequency of a bosonic spectral function, the real-frequency solver should yield improved self-consistent predictions at both zero and finite frequency. Finally, the Keldysh formulation can describe genuine out-of-equilibrium dynamics where the fluctuation-dissipation relation (10) is no longer satisfied [20], and it will be interesting to find self-consistent solutions for the transient evolution after a quantum quench.

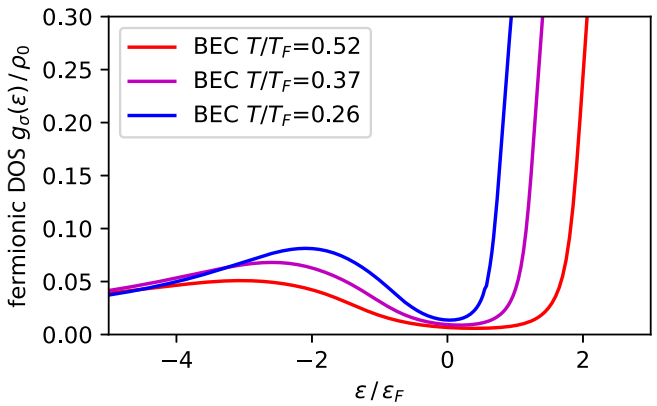

FIG. 6. Fermionic density of states $g_\sigma(\varepsilon)$ vs frequency ε on the BEC side $\beta E_b = 8$ ($1/k_F a \simeq 1$). The DOS is strongly suppressed in a region of width $2|\mu|$ around the chemical potential. The DOS is given in units of the ideal Fermi gas DOS at zero temperature, $\rho_0 = g_\sigma^{(0)} = mk_F/2\pi^2$.

Note added. Recently, two other studies appeared which compute spectral functions in real frequency using Fourier transforms [26] and spectral representations [44].

ACKNOWLEDGMENTS

We acknowledge discussions with E. Dizer, B. Frank, K. Fujii, E. Gull, J. Lang, G. Möller, J. Pawlowski, F. Werner, D. Zgid, and W. Zwerger and thank J. Lang for sharing spectral data. This work was supported by the Deutsche Forschungsgemeinschaft (German Research Foundation), Project No. 273811115 (SFB1225 ISOQUANT) and under Germany's Excellence Strategy EXC2181/1-390900948 (the Heidelberg STRUCTURES Excellence Cluster).

APPENDIX: LEADING-ORDER SELF-ENERGIES IN THE VIRIAL EXPANSION

Beyond the vacuum limit, the fermionic self-energy arises at $O(z)$. To leading order, one can replace the fermionic occupation $f(x-\mu) = ze^{-\beta x} + O(z^2)$ and neglect the bosonic occupation $b(y-2\mu) = O(z^2)$. For the first-order self-energy it is thus sufficient to use the zeroth-order Green's functions G^R_{p0} and $A_{\sigma 0}(\boldsymbol{p}', \varepsilon') = \delta(\varepsilon' + \mu - \varepsilon_{p'})$ such that Eq. (12) simplifies to

$$\Sigma^{(1)R}_\sigma(\boldsymbol{p}, \varepsilon = \varepsilon_{\boldsymbol{p}} - \mu + s, a^{-1}) = z\int_{\boldsymbol{p}'} e^{-\beta\varepsilon_{p'}} G^R_{p0}(\boldsymbol{p}+\boldsymbol{p}', \varepsilon + \varepsilon_{p'} - \mu) = z\frac{4\pi}{m}\int_{\boldsymbol{p}'} \frac{e^{-\beta\varepsilon_{p'}}}{a^{-1} - \sqrt{-m\left(s + \frac{1}{2}\varepsilon_{\boldsymbol{p}-\boldsymbol{p}'} + i0\right)}}. \tag{A1}$$

The fermion spectral parameter $s = \varepsilon + \mu - \varepsilon_{\boldsymbol{p}}$ denotes the shift away from the fermion shell, which is located at $s = 0$. Analytical expressions for the first-order self-energy $\Sigma^{(1)R}_\sigma(\boldsymbol{p}, s, a^{-1})$ are available if only one of the three parameters p, s, and a^{-1} is nonzero:

$$\Sigma^{(1)R}_\sigma(\boldsymbol{p}, 0, a^{-1} \to 0) = \frac{2zT}{\sqrt{\pi}}\left(-\frac{4a^{-1}}{\sqrt{2mT}}\frac{F_D(p/\sqrt{2mT})}{p/\sqrt{2mT}} - i\frac{\operatorname{erf}(p/\sqrt{2mT})}{p/\sqrt{2mT}}\right), \tag{A2}$$

$$\Sigma^{(1)R}_\sigma(0, s, 0) = -i\frac{2zT}{\sqrt{\pi}}U(\tfrac{1}{2}, 0, 2s/T + i0), \tag{A3}$$

$$\Sigma^{(1)R}_\sigma(0, 0, a^{-1}) = i\frac{8zT}{\pi^2}\frac{a^{-2}}{2mT}G\left(\left((1, \tfrac{3}{2}, 2), ()\right), \left((\tfrac{3}{2}, 2), ()\right), i\frac{\sqrt{2mT}}{2a^{-1}}, \tfrac{1}{2}\right), \tag{A4}$$

$$\Sigma^{(1)R}_\sigma(0, -E_b, a^{-1}) = -i\frac{2zT}{\sqrt{\pi}}G\left(((), (\tfrac{3}{2})), ((0, 1), ()), 2/a^2mT\right) + \text{real part}. \tag{A5}$$

Here F_D denotes the Dawson, U the hypergeometric, and G the Meijer function. The unitary on-shell self-energy (A2) was given in [36], and specifically $\Sigma^{(1)R}_\sigma(0,0,0) = -i4zT/\pi$. Additionally, the bound-state contribution for all argument values is given analytically to $O(z)$ by

$$\operatorname{Im}\Sigma^{(1)bR}_\sigma(\boldsymbol{p}, s, a^{-1} > 0) = -2zT\Theta(a)\Theta(-s - E_b)\sqrt{2E_b/T}\frac{e^{-(\bar{p}-\bar{p}')^2} - e^{-(\bar{p}+\bar{p}')^2}}{4\bar{p}}, \tag{A6}$$

with $\bar{p} = p/\sqrt{2mT}$ and $\bar{p}' = \sqrt{-2(s+E_b)/T}$, and the last ratio becomes $\bar{p}'\exp(-\bar{p}'^2)$ in the limit $\bar{p} \to 0$. These analytical forms serve as a benchmark for the accuracy of the numerical solution at small z.

[1] I. Bloch, J. Dalibard, and W. Zwerger, Many-body physics with ultracold gases, Rev. Mod. Phys. **80**, 885 (2008).

[2] S. Giorgini, L. P. Pitaevskii, and S. Stringari, Theory of ultracold Fermi gases, Rev. Mod. Phys. **80**, 1215 (2008).

[3] G. C. Strinati, P. Pieri, G. Röpke, P. Schuck, and M. Urban, The BCS-BEC crossover: From ultra-cold Fermi gases to nuclear systems, Phys. Rep. **738**, 1 (2018).

[4] X. Li, S. Wang, X. Luo, Y.-Y. Zhou, K. Xie, H.-C. Shen, Y.-Z. Nie, Q. Chen, H. Hu, Y.-A. Chen, X.-C. Yao, and J.-W. Pan, Observation and quantification of pseudogap in unitary Fermi gases, arXiv:2310.14024.

[5] *The BCS-BEC Crossover and the Unitary Fermi Gas*, edited by W. Zwerger, Lecture Notes in Physics Vol. 836 (Springer, Berlin, 2012).

[6] P. Nozières and S. Schmitt-Rink, Bose condensation in an attractive fermion gas: From weak to strong coupling superconductivity, J. Low Temp. Phys. **59**, 195 (1985).

[7] C. A. R. Sá de Melo, M. Randeria, and J. R. Engelbrecht, Crossover from BCS to Bose superconductivity: Transition temperature and time-dependent Ginzburg-Landau theory, Phys. Rev. Lett. **71**, 3202 (1993).

[8] A. Perali, P. Pieri, G. C. Strinati, and C. Castellani, Pseudogap and spectral function from superconducting fluctuations to the bosonic limit, Phys. Rev. B **66**, 024510 (2002).

[9] L. P. Gor'kov and T. K. Melik-Barkhudarov, Contribution to the theory of super-fluidity in an imperfect Fermi gas, Zh. Eksp. Teor. Fiz. **40**, 1452 (1961).

[10] M. J. H. Ku, A. T. Sommer, L. W. Cheuk, and M. W. Zwierlein, Revealing the superfluid lambda transition in the universal thermodynamics of a unitary Fermi gas, Science **335**, 563 (2012).

[11] E. Burovski, N. Prokof'ev, B. Svistunov, and M. Troyer, Critical temperature and thermodynamics of attractive fermions at unitarity, Phys. Rev. Lett. **96**, 160402 (2006).

[12] R. Haussmann, W. Rantner, S. Cerrito, and W. Zwerger, Thermodynamics of the BCS-BEC crossover, Phys. Rev. A **75**, 023610 (2007).

[13] R. Hanai and Y. Ohashi, Self-consistent T-matrix approach to an interacting ultracold Fermi gas with mass imbalance, J. Low Temp. Phys. **175**, 272 (2014).

[14] B. Frank, J. Lang, and W. Zwerger, Universal phase diagram and scaling functions of imbalanced Fermi gases, J. Exp. Theor. Phys. **127**, 812 (2018).

[15] M. Pini, P. Pieri, and G. C. Strinati, Fermi gas throughout the BCS-BEC crossover: Comparative study of t-matrix approaches with various degrees of self-consistency, Phys. Rev. B **99**, 094502 (2019).

[16] C.-N. Yeh, S. Iskakov, D. Zgid, and E. Gull, Fully self-consistent finite-temperature *GW* in Gaussian Bloch orbitals for solids, Phys. Rev. B **106**, 235104 (2022).

[17] K. Van Houcke, F. Werner, E. Kozik, N. Prokof'ev, B. Svistunov, M. J. H. Ku, A. T. Sommer, L. W. Cheuk, A. Schirotzek, and M. W. Zwierlein, Feynman diagrams versus Fermi-gas Feynman emulator, Nat. Phys. **8**, 366 (2012).

[18] S. Sachdev, *Quantum Phase Transitions* (Cambridge University Press, Cambridge, 1999).

[19] T. Enss, Quantum critical transport in the unitary Fermi gas, Phys. Rev. A **86**, 013616 (2012).

[20] A. Kamenev, *Field Theory of Non-Equilibrium Systems* (Cambridge University Press, Cambridge, 2011).

[21] A. A. Abrikosov, L. P. Gorkov, and I. E. Dzyaloshinski, *Methods of Quantum Field Theory in Statistical Physics* (Dover, Mineola, 1975).

[22] T. Kawamura, R. Hanai, D. Kagamihara, D. Inotani, and Y. Ohashi, Nonequilibrium strong-coupling theory for a driven-dissipative ultracold Fermi gas in the BCS-BEC crossover region, Phys. Rev. A **101**, 013602 (2020).

[23] G. Baym, Self-consistent approximations in many-body systems, Phys. Rev. **127**, 1391 (1962).

[24] R. Haussmann, Crossover from BCS superconductivity to Bose-Einstein condensation: A self-consistent theory, Z. Phys. B **91**, 291 (1993).

[25] K. Fujii and T. Enss, Bulk viscosity of resonantly interacting fermions in the quantum virial expansion, Ann. Phys. (NY) **453**, 169296 (2023).

[26] C. H. Johansen, B. Frank, and J. Lang, preceding paper, Spectral functions of the strongly interacting three-dimensional Fermi gas, Phys. Rev. A **109**, 023324 (2024).

[27] P. A. Murthy, M. Neidig, R. Klemt, L. Bayha, I. Boettcher, T. Enss, M. Holten, G. Zürn, P. M. Preiss, and S. Jochim, High-temperature pairing in a strongly interacting two-dimensional Fermi gas, Science **359**, 452 (2018).

[28] R. Haussmann, M. Punk, and W. Zwerger, Spectral functions and rf response of ultracold fermionic atoms, Phys. Rev. A **80**, 063612 (2009).

[29] R. Schmidt and T. Enss, Excitation spectra and rf response near the polaron-to-molecule transition from the functional renormalization group, Phys. Rev. A **83**, 063620 (2011).

[30] J. Levinsen and M. M. Parish, Strongly Interacting two-dimensional Fermi gases, in *Annual Review of Cold Atoms and Molecules*, edited by K. W. Madison, K. Bongs, L. D. Carr, A. M. Rey, and H. Zhai (World Scientific, Singapore, 2015), Vol. 3, Chap. 1, pp. 1–75.

[31] M. Bauer, M. M. Parish, and T. Enss, Universal equation of state and pseudogap in the two-dimensional Fermi gas, Phys. Rev. Lett. **112**, 135302 (2014).

[32] J. Hofmann, Quantum anomaly, universal relations, and breathing mode of a two-dimensional Fermi gas, Phys. Rev. Lett. **108**, 185303 (2012).

[33] P. A. Murthy, N. Defenu, L. Bayha, M. Holten, P. M. Preiss, T. Enss, and S. Jochim, Quantum scale anomaly and spatial coherence in a 2D Fermi superfluid, Science **365**, 268 (2019).

[34] P. Massignan, G. M. Bruun, and H. Smith, Viscous relaxation and collective oscillations in a trapped Fermi gas near the unitarity limit, Phys. Rev. A **71**, 033607 (2005).

[35] T. Enss, R. Haussmann, and W. Zwerger, Viscosity and scale invariance in the unitary Fermi gas, Ann. Phys. (NY) **326**, 770 (2011).

[36] K. Dusling and T. Schäfer, Bulk viscosity and conformal symmetry breaking in the dilute Fermi gas near unitarity, Phys. Rev. Lett. **111**, 120603 (2013).

[37] T. Enss, Bulk viscosity and contact correlations in attractive Fermi gases, Phys. Rev. Lett. **123**, 205301 (2019).

[38] Y. Nishida, Viscosity spectral functions of resonating fermions in the quantum virial expansion, Ann. Phys. (NY) **410**, 167949 (2019).

[39] J. Hofmann, High-temperature expansion of the viscosity in interacting quantum gases, Phys. Rev. A **101**, 013620 (2020).

[40] M. Braby, J. Chao, and T. Schäfer, Thermal conductivity and sound attenuation in dilute atomic Fermi gases, Phys. Rev. A **82**, 033619 (2010).

[41] B. Frank, W. Zwerger, and T. Enss, Quantum critical thermal transport in the unitary Fermi gas, Phys. Rev. Res. **2**, 023301 (2020).

[42] T. Enss and R. Haussmann, Quantum mechanical limitations to spin transport in the unitary Fermi gas, Phys. Rev. Lett. **109**, 195303 (2012).

[43] T. Enss and J. H. Thywissen, Universal spin transport and quantum bounds for unitary fermions, Annu. Rev. Condens. Matter Phys. **10**, 85 (2019).

[44] E. Dizer, J. Horak, and J. M. Pawlowski, Spectral properties and observables in ultracold Fermi gases, arXiv:2311.16788.